

# Intrinsic Anomalous Hall Effect in a Bosonic Chiral Superfluid

Guan-Hua Huang,<sup>1,2</sup> Zhi-Fang Xu,<sup>1,2,3,4,\*</sup> and Zhigang Wu<sup>2,3,4,†</sup>

<sup>1</sup>*Department of Physics, Southern University of Science and Technology, Shenzhen, 518055, China*

<sup>2</sup>*Shenzhen Institute for Quantum Science and Engineering,  
Southern University of Science and Technology, Shenzhen 518055, China.*

<sup>3</sup>*International Quantum Academy, Shenzhen 518048, China.*

<sup>4</sup>*Guangdong Provincial Key Laboratory of Quantum Science and Engineering,  
Southern University of Science and Technology, Shenzhen 518055, China.*

(Dated: July 6, 2022)

The anomalous Hall effect has had a profound influence on the understanding of many electronic topological materials but is much less studied in their bosonic counterparts. We predict that an intrinsic anomalous Hall effect exists in a recently realized bosonic chiral superfluid, a  $p$ -orbital Bose-Einstein condensate in a 2D hexagonal boron nitride optical lattice [X. Wang *et al.*, *Nature (London)* **596**, 227 (2021)]. We evaluate the frequency-dependent Hall conductivity within a multi-orbital Bose-Hubbard model that accurately captures the real experimental system. We find that in the high frequency limit, the Hall conductivity is determined by finite loop current correlations on the  $s$ -orbital residing sublattice, the latter a defining feature of the system's chirality. In the opposite limit, the dc Hall conductivity can trace its origin back to the non-interacting band Berry curvature at the condensation momentum, although the contribution from atomic interactions can be significant. We discuss available experimental probes to observe this intrinsic anomalous Hall effect at both zero and finite frequencies.

*Introduction.*—The capacity of ultracold atomic gases as quantum simulators of more complex condensed matter systems owes to the plethora of experimental tools available to provide these neutral atoms with solid-state-like settings [1–3]. Well-known examples include optical lattice potentials [4, 5], synthetic spin-orbit couplings [6–8] and artificial gauge fields [9, 10]. Motivated by the desire to simulate electronic systems for which orbital degrees of freedom are essential [11], experimentalists have begun to load atoms onto higher Bloch bands of optical lattices of various crystal structures [12–23]. With the choice of bosonic atoms, this experimental approach has also led to the creation of novel atomic superfluids [15–18, 22, 23] which, among other things, exhibit a spontaneous breaking of time-reversal symmetry (TRS) due to atomic interactions.

The recently realized  $p$ -orbital Bose-Einstein condensate in a 2D boron nitride optical lattice [23] is a particularly interesting example of such superfluids. A prominent feature of this system is that it acquires a macroscopic angular momentum in the absence of any artificial magnetic field or rotation of the trapping potential, and displays a chirality akin to that of superfluid  $^3\text{He}$  [24, 25]. Furthermore, it contains a topologically non-trivial quasi-particle band structure as well as gapless edge states, both reminiscent of similar concepts in fermionic topological materials [26]. Because the Hall response often plays a fundamental role in understanding and characterizing these topological materials [27–29], it is only natural to ask if an anomalous Hall effect, quantum or otherwise, exists in their newly discovered bosonic counterpart.

In electronic materials, the intrinsic (scattering-free) anomalous Hall effect and its quantum version are both well understood in terms of the geometrical properties of

the topologically non-trivial band structures [30, 31]. In this framework, the dc Hall conductivity is determined by the summation of Berry curvatures of the occupied Bloch states, weighted by the Fermi-Dirac distribution function [31]. This means that anomalous Hall responses can also occur in bosonic quantum gases if the atoms are excited to states having non-zero Berry curvature, either in a non-equilibrium situation [32, 33] or at finite temperatures [34, 35]. At zero temperature, however, earlier studies found vanishing dc Hall responses in bosonic models for both topologically trivial [33] and non-trivial [35] band structures.

In addition to the dc Hall response, the ac anomalous Hall effect, i.e., the frequency-dependent Hall response, has been widely studied in chiral superconductors in the context of the Kerr effect [36–40]. There, the Hall response originates not from a topologically non-trivial band structure but rather from the TRS-breaking superconductivity. In particular, a remarkable relation is found between the high-frequency Hall response and the loop current correlations [39]. The dc Hall conductivity in those systems, however, cannot be directly related to the Berry curvatures of the electronic bands [37].

In this paper, we show that an intrinsic anomalous Hall effect indeed exists in the bosonic chiral superfluid at zero temperature, for both zero and finite frequencies. Fascinatingly, both of the physical mechanisms aforementioned are at play in our system. At high frequencies, we found a striking similarity to the chiral superconductors in that the Hall response appears as a consequence of the chirality. The dc Hall conductivity, on the other hand, can still be understood in terms of the Berry curvature of the non-interacting bands, although the effect of atomic interactions needs to be accounted for. We will discuss

experimental methods uniquely suitable to detecting the anomalous Hall effect in this ultracold atomic system.

*Bosonic chiral superfluid*— The atomic chiral superfluid is realized in a quasi-2D  $^{87}\text{Rb}$  gas confined in a hexagonal boron nitride (BN) optical lattice [23]. The BN lattice is formed by superimposing two sets of triangular lattice potential  $A$  and  $B$ , spanned by primitive vectors  $\mathbf{a}_1 = a(\sqrt{3}/2, -1/2)$  and  $\mathbf{a}_2 = a(\sqrt{3}/2, 1/2)$ , where  $a$  is the lattice constant (see Fig. 1(a)). The local potential wells on  $B$  sublattice sites are deeper than those on  $A$ , such that the energy of the  $s$ -orbital on  $A$  sites is comparable to that of the two degenerate  $p$ -orbitals on  $B$ . In such a case, these three orbitals form a subspace in which an effective multi-orbital Bose-Hubbard model can be constructed to describe the system with the Hamiltonian  $\hat{H} = \hat{H}_0 + \hat{H}_{\text{int}}$ , where the kinetic and interaction energy are given by [41]

$$\hat{H}_0 = \sum_{\mathbf{r}} \epsilon_s \hat{s}_{\mathbf{r}}^\dagger \hat{s}_{\mathbf{r}} + \sum_{\mathbf{r}, \alpha} \epsilon_p \hat{p}_{\alpha, \mathbf{r}}^\dagger \hat{p}_{\alpha, \mathbf{r}} + \sum_{\mathbf{r}, \alpha, l} (t_l^\alpha \hat{s}_{\mathbf{r}}^\dagger \hat{p}_{\alpha, \mathbf{r} + \delta_l} + h.c.)$$

and

$$\hat{H}_{\text{int}} = \frac{U_s}{2} \sum_{\mathbf{r}} \hat{s}_{\mathbf{r}}^\dagger \hat{s}_{\mathbf{r}}^\dagger \hat{s}_{\mathbf{r}} \hat{s}_{\mathbf{r}} + \frac{U_p}{2} \sum_{\mathbf{r}, \alpha \alpha' \beta \beta'} \hat{p}_{\alpha', \mathbf{r}}^\dagger \hat{p}_{\beta', \mathbf{r}}^\dagger \hat{p}_{\beta, \mathbf{r}} \hat{p}_{\alpha, \mathbf{r}}$$

respectively. Here in the second term of  $\hat{H}_{\text{int}}$  only the angular momentum conserving processes are retained in the summation. In addition, throughout the paper, summation over the lattice vector  $\mathbf{r}$  is understood to be restricted to  $A$  sublattice for  $s$ -orbital and to  $B$  sublattice for  $p$ -orbitals. Thus,  $\hat{s}_{\mathbf{r}}^\dagger$  creates a  $s$ -orbital atom with energy  $\epsilon_s$  on lattice site  $\mathbf{r} \in A$ . The two degenerate  $p$ -orbitals with energy  $\epsilon_p$ , created by  $\hat{p}_{\alpha, \mathbf{r}}^\dagger$  ( $\alpha = \pm$ ) on site  $\mathbf{r} \in B$ , are eigenstates of the rotation operator and thus time-reversed counterparts of each other. The nearest neighbor hopping parameter along the vector  $\delta_l$  ( $l = 1, 2, 3$ ) can be written as  $t_l^\pm = t_l^{\mp*} = t e^{i(l-1)2\pi/3}$  due to the phase winding of the  $p$ -orbitals and the  $C_3$  symmetry of the lattice. The on-site interaction strengths for  $s$  and  $p$ -orbitals,  $U_s$  and  $U_p$  respectively, are both proportional to the scattering length of the atoms. All these parameters can be controlled and determined precisely in experiments, allowing for quantitative comparisons between theoretical and experimental studies.

The non-interacting band dispersion  $\epsilon_n(\mathbf{k})$  ( $n = 0, 1, 2$ ), as shown in Fig 1(b), can be solved analytically by diagonalizing

$$h_0(\mathbf{k}) \equiv \begin{pmatrix} \epsilon_s & f_{\mathbf{k}}^+ & f_{\mathbf{k}}^- \\ \epsilon_p & 0 & 0 \\ h.c. & \epsilon_p & \end{pmatrix}, \quad (1)$$

where  $f_{\mathbf{k}}^\pm = \sum_l t_l^\pm e^{i\mathbf{k} \cdot \delta_l}$ . Since the Hamiltonian preserves the time-reversal symmetry, the dispersion has the property  $\epsilon_n(\mathbf{k}) = \epsilon_n(-\mathbf{k})$ . In addition, the local minima of

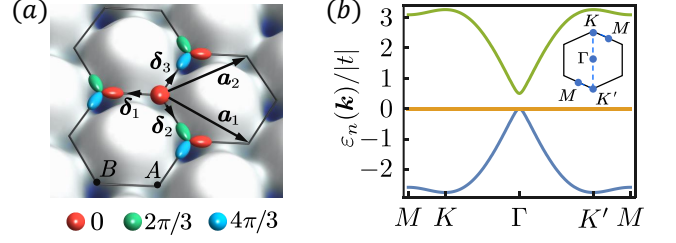


FIG. 1. (a) Illustration of the boron nitride lattice potential, where the atoms reside in the  $s$ -orbital on  $A$  sites and in the two degenerate  $p$ -orbitals on  $B$  sites. The colors indicate the phase winding of the  $s$  and  $p$ -orbital wave functions. (b) Non-interacting band dispersions of the BN lattice described by  $h_0$  in Eq. (1), for  $\epsilon_s - \epsilon_p = 0.5|t|$ . Note that there is a band touching point at  $\Gamma$ . The inset depicts the first Brillouin zone and shows the path along which the dispersions are plotted.

the bottom band occur at the time-reversed pair of momenta  $\mathbf{K}$  and  $\mathbf{K}'$ , as can be seen from the band dispersion  $\epsilon_0(\mathbf{k}) = \frac{1}{2}[\epsilon_s + \epsilon_p - \sqrt{(\epsilon_s - \epsilon_p)^2 + 4(|f_{\mathbf{k}}^+|^2 + |f_{\mathbf{k}}^-|^2)}]$ .

At zero temperature, a mean-field analysis shows that the presence of weak interactions leads to the condensation of atoms into either  $\mathbf{K}$  or  $\mathbf{K}'$  in the momentum space, spontaneously breaking the time-reversal symmetry. It can be further shown by symmetry considerations that the  $\mathbf{K}$  ( $\mathbf{K}'$ ) ground state corresponds to the condensation of atoms into pure  $p_+$  ( $p_-$ ) orbital on  $B$  sublattice sites [41]. Taken together, the condensate wave function associated with  $\mathbf{K} = \frac{4\pi}{3a}(0, 1)$  condensation can be written as

$$\langle \hat{\psi}_{\mathbf{k}} \rangle = \sqrt{N} (\cos \xi \quad \sin \xi \quad 0)^T \delta_{\mathbf{k}, \mathbf{K}}. \quad (2)$$

Here we adopt a spinor notation  $\hat{\psi}_{\mathbf{k}} \equiv (\hat{s}_{\mathbf{k}} \quad \hat{p}_{+, \mathbf{k}} \quad \hat{p}_{-, \mathbf{k}})^T$  where  $\hat{s}_{\mathbf{k}} = \frac{1}{\sqrt{N_u}} \sum_{\mathbf{r}} e^{-i\mathbf{k} \cdot \mathbf{r}} \hat{s}_{\mathbf{r}}$  with  $N_u$  as the number of unit cells;  $N$  is the number of atoms, and  $\xi$  is determined by minimizing the Gross-Pitaevskii energy [41]. The key property that distinguishes this multi-orbital superfluid from many of the previously realized atomic superfluids is that it is globally chiral, carrying a total angular momentum of  $\langle \hat{L}_z \rangle = \hbar \sum_{\mathbf{r}} \langle \hat{p}_{+, \mathbf{r}}^\dagger \hat{p}_{+, \mathbf{r}} - \hat{p}_{-, \mathbf{r}}^\dagger \hat{p}_{-, \mathbf{r}} \rangle = N \hbar (\sin \xi)^2$ .

*Anomalous Hall effect*— We first demonstrate the anomalous Hall effect by evaluating the frequency-dependent Hall conductivity using the Kubo formula

$$\sigma_H(\omega) \equiv \frac{1}{\mathcal{A}\omega} \text{Im} \chi_{x,y}^J(\omega), \quad (3)$$

where  $\mathcal{A}$  is the system's area, and  $\chi_{x,y}^J(\omega)$  is the Fourier transform of the retarded current-current correlation function  $\chi_{x,y}^J(t-t') = -i\hbar^{-1} \theta(t-t') \langle [\hat{J}_x(t), \hat{J}_y(t')] \rangle$ . In our tight-binding model, the total current operator takes the familiar form of

$$\hat{\mathbf{J}} = \frac{i}{\hbar} \sum_{\mathbf{r}, l} [\delta_l (t_l^+ \hat{s}_{\mathbf{r}}^\dagger \hat{p}_{+, \mathbf{r} + \delta_l} + t_l^- \hat{s}_{\mathbf{r}}^\dagger \hat{p}_{-, \mathbf{r} + \delta_l}) - h.c.]. \quad (4)$$

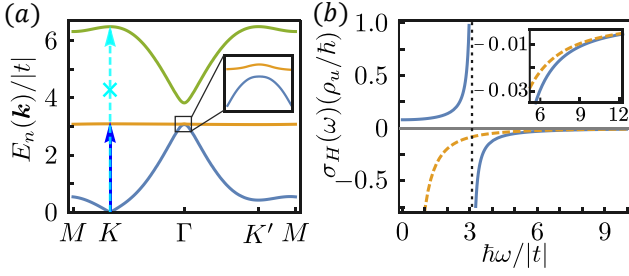


FIG. 2. (a) Bogoliubov spectrum of the chiral superfluid. The inset shows an expanded view of a small gap opening at the  $\Gamma$  point. The arrow with the solid line indicates the transition from the ground state to the first excitation band at  $\mathbf{K}$  in the presence of an “electric field”; the arrow with the dashed line indicates the absence of such transitions to the second excitation band. (b) Frequency-dependent Hall conductivity. The dashed line shows the asymptotic behavior of  $\sigma_H(\omega)$  given by Eq. (12). The inset is an expanded view of this asymptotic behavior. Here  $\epsilon_s - \epsilon_p = 0.5|t|$ ,  $\rho_u U_s = 1.2|t|$  and  $\rho_u U_p = 0.72|t|$ .

To calculate the Hall conductivity we need first to determine the collective excitations, which can be found by solving the Bogliubov-de Gennes equation

$$\tau_z \mathcal{H}_B(\mathbf{k}) V_n(\mathbf{k}) = E_n(\mathbf{k}) V_n(\mathbf{k}). \quad (5)$$

Here  $\tau_z = \sigma_z \otimes I$ , where  $\sigma_z$  is the Pauli matrix and  $I$  is the  $3 \times 3$  identity matrix;  $E_n(\mathbf{k})$  is the Bogoliubov spectrum,  $V_n(\mathbf{k})$  is the corresponding amplitude with the normalization  $V_n^\dagger(\mathbf{k}) \tau_z V_n(\mathbf{k}) = \tau_z$  and the matrix  $\mathcal{H}_B(\mathbf{k})$  (assuming the  $\mathbf{K}$  condensation) is given by

$$\mathcal{H}_B(\mathbf{k}) = \begin{pmatrix} h_0(\mathbf{k}) + g - \mu I & g' \\ g' & h_0^*(2\mathbf{K} - \mathbf{k}) + g - \mu I \end{pmatrix} \quad (6)$$

where  $g = \text{diag}(2U_s \rho_u \cos^2 \xi, 2U_p \rho_u \sin^2 \xi, 2U_p \rho_u \sin^2 \xi)$  and  $g' = \text{diag}(U_s \rho_u \cos^2 \xi, U_p \rho_u \sin^2 \xi, 0)$  are diagonal matrices accounting for the atomic interactions,  $\rho_u$  is the number of atoms per unit cell and  $\mu$  is the chemical potential. Shown in Fig. 2(a) is a typical plot of the Bogoliubov spectrum obtained from Eq. (5). As usual the full solutions to Eq. (5) include both the positive ( $n = 0, 1, 2$ ) and negative ( $n = \bar{0}, \bar{1}, \bar{2}$ ) branches, but only the former are physically relevant and shown in the figure. Importantly, the condensate wave function is contained in the eigenvector corresponding to  $E_0(\mathbf{K})$ , namely  $V_0(\mathbf{K}) = (1/\sqrt{2})(\Phi - \Phi^*)^T$  where  $\Phi = (\cos \xi \ \sin \xi \ 0)$ . It’s also worth noting that a small gap opens at the  $\Gamma$  point, which renders the Bogoliubov excitations topological [23, 42].

Within the Bogoliubov framework, the Hall conductivity defined in Eq. (3) is given by

$$\sigma_H(\omega) = \frac{N}{\mathcal{A} \hbar^2} \text{Im} \sum_{n=1,2} \left[ \frac{J_{x,0n}(\mathbf{K}) J_{y,n0}(\mathbf{K})}{\hbar \omega - E_n(\mathbf{K}) + E_0(\mathbf{K}) + i0^+} - \frac{J_{y,0n}(\mathbf{K}) J_{x,n0}(\mathbf{K})}{\hbar \omega + E_n(\mathbf{K}) - E_0(\mathbf{K}) + i0^+} \right], \quad (7)$$

where  $J_{i,0n}(\mathbf{K}) = \sqrt{2} V_0^\dagger(\mathbf{K}) \partial_i \mathcal{H}_B(\mathbf{K}) V_n(\mathbf{K})$  with  $\partial_i \equiv \partial/\partial k_i$ . The Hall conductivity calculated from Eq. (7) is plotted in Fig. 2(b). From the expression we see that the finite Hall conductivity comes from the inter-band transitions at momentum  $\mathbf{K}$  when an “electric field” is applied to the system. Here it is critical that the condensation occurs at a momentum for which the velocity operator  $\nabla_{\mathbf{k}} \mathcal{H}_B(\mathbf{k})$  is finite; otherwise no inter-band transitions would take place and hence no anomalous Hall effect [33, 35]. Another notable aspect is that the second excitation band does not contribute to the conductivity as a result of the selection rule  $J_{i,02} = 0$ . This explains why only one singularity, located at  $\hbar \omega = E_1(\mathbf{K}) - E_0(\mathbf{K})$ , appears in the plot of  $\sigma_H(\omega)$  in Fig. 2(b). This selection rule reflects some of the general properties of the high-symmetry point  $\mathbf{K}$  in the Brillouin zone, valid beyond our tight-binding model [41]. More specifically, at this momentum the current operator involves only the coupling between the  $s$  and  $p_-$  orbitals while the wave functions of both the condensate and the second Bogoliubov excitation contain a mixture of the  $s$  and  $p_+$  orbitals; hence no transitions between them. To understand other features of  $\sigma_H(\omega)$  and the physical reasons underlying the anomalous Hall effect, we next analyze both the high and low frequency limit of the Hall response.

*High frequency Hall response and loop current correlations.*—In the high frequency limit  $\hbar \omega \gg |t|$ , it can be shown from the Kubo formula definition of the Hall conductivity that [43]

$$\sigma_H(\omega) = \frac{1}{\hbar \mathcal{A} \omega^2} \text{Im} \langle [\hat{J}_x, \hat{J}_y] \rangle + O\left(\frac{1}{\omega^4}\right). \quad (8)$$

Using Eq. (4) to evaluate the above commutator we find that in this limit

$$\sigma_H(\omega) = \frac{|t|^2}{3N_u \hbar^3 \omega^2} \left( \langle \hat{C}_s \rangle + \sum_{\alpha\alpha'} \langle \hat{C}_p^{\alpha\alpha'} \rangle \right), \quad (9)$$

where  $\hat{C}_s$  and  $\hat{C}_p^{\alpha\alpha'}$  are the loop current correlators

$$\hat{C}_s = i \sum_{\mathbf{r}, \langle ll' \rangle} (e^{i\pi} \hat{s}_{\mathbf{r}-\delta_l}^\dagger \hat{s}_{\mathbf{r}-\delta_{l'}} - h.c.); \quad (10)$$

$$\hat{C}_p^{\alpha\alpha'} = i \sum_{\mathbf{r}, \langle ll' \rangle} (e^{i\theta_{ll'}^{\alpha\alpha'}} \hat{p}_{\alpha', \mathbf{r}+\delta_{l'}}^\dagger \hat{p}_{\alpha, \mathbf{r}+\delta_l} - h.c.). \quad (11)$$

Here  $\langle ll' \rangle$  denotes the summation over the cyclic permutations (12);(23);(31),  $\theta_{ll'}^{++} = -\theta_{ll'}^{--} = -\mathbf{K} \cdot (\delta_l - \delta_{l'})$  and  $\theta_{ll'}^{+-} = -\theta_{ll'}^{-+} = -\mathbf{K} \cdot (\delta_l + \delta_{l'})$ . We note that  $\hat{C}_s$  is defined on sets of three nearest-neighbor  $A$  sites, each set encircling a  $p$ -orbital residing  $B$  site as illustrated in Fig. 3(a); similarly  $\hat{C}_p^{\alpha\alpha'}$  are defined along the triangles encircling the  $s$ -orbital residing  $A$  sites. These correlators are so named because, were we to include nearest neighbor hoppings within each sublattice, the loop current is

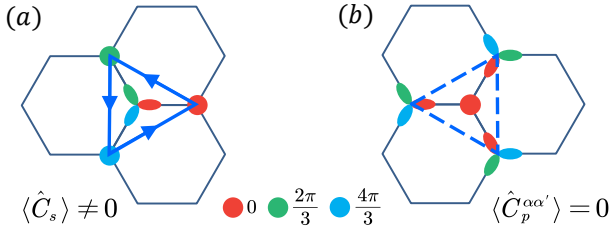


FIG. 3. (a) Finite loop current correlation on the  $s$ -orbital residing  $A$  sublattice. (b) Vanishing loop current correlations on the  $p$ -orbital residing  $B$  sublattice.

given by  $\hat{J}_{loop} = -a(|t_s|\hat{C}_s + \sum_{\alpha\alpha'}|t_p^{\alpha\alpha'}|\hat{C}_p^{\alpha\alpha'})$ , where  $|t_s|$  and  $|t_p^{\alpha\alpha'}|$  are the nearest neighbor hopping strengths within  $A$  and  $B$  sublattices respectively [41]. Relations analogous to Eq. (9) were first discussed in models of spin-singlet chiral  $d$ -wave superconductors [39].

Now Eq. (9) allows us to see the connection between the chirality of the system and the high frequency Hall response. As discussed earlier, the superfluid's chirality arises from the condensation of atoms in the  $p_+$  orbitals on the  $B$  sublattice, which effectively creates a vortex lattice. Thus we expect a finite loop current correlation when the loops encircle the vortex cores and a vanishing correlation when they do not (see Fig. 3). Indeed, using the ground state wave function in Eq. (2) we find that  $\langle \hat{C}_s \rangle = -3\sqrt{3}N(\cos \xi)^2$  and  $\langle \hat{C}_p^{\alpha\alpha'} \rangle = 0$ , which leads to

$$\sigma_H(\omega) = -\frac{\sqrt{3}\rho_u|t|^2}{\hbar^3\omega^2}(\cos \xi)^2 \quad (12)$$

for  $\hbar\omega \gg |t|$ . This result is plotted in Fig. 2(b) and agrees well with the exact calculation in the high frequency limit.

*dc Hall response and Berry curvature.*—At low frequencies, the first thing to note is the general property that  $\sigma_H(\omega)$  is an even function of  $\omega$ , which means that  $\lim_{\omega \rightarrow 0} \sigma_H(\omega) = \sigma_H(0) + O(\omega^2)$ . This explains the small deviations of  $\sigma_H(\omega)$  from  $\sigma_H(0)$  for a significant range of frequency. Next we explore the connections between the dc Hall conductivity  $\sigma_H(0)$  and the Berry curvatures of the non-interacting and the Bogoliubov excitation bands. The Berry curvature of the latter is given by [44, 45]

$$\Omega_n(\mathbf{k}) = i\epsilon_{ij} \sum_{m \neq n} \frac{V_n^\dagger \partial_i \mathcal{H}_B V_m \tau_{z,mm} V_m^\dagger \partial_j \mathcal{H}_B V_n}{(E_n - E_m)^2}, \quad (13)$$

where  $\epsilon_{ij}$  is the Levi-Civita symbol and repeated  $i, j$  indices are summed over. In contrast to Eq. (7), the summation over the band index here includes both the positive ( $n = 0, 1, 2$ ) and negative ( $n = \bar{0}, \bar{1}, \bar{2}$ ) branches, which are related to each other by  $E_n(\mathbf{k}) = -E_{\bar{n}}(2\mathbf{K} - \mathbf{k})$ . Since  $n = 0, \mathbf{k} = \mathbf{K}$  and  $n = \bar{0}, \mathbf{k} = \mathbf{K}$  denote the same ground state, the dispersions  $E_0(\mathbf{k})$  and  $E_{\bar{0}}(\mathbf{k})$  are joined at  $\mathbf{k} = \mathbf{K}$ , giving rise to a band touching point in the spectrum of  $\mathcal{H}_B$ . As a result the formula in

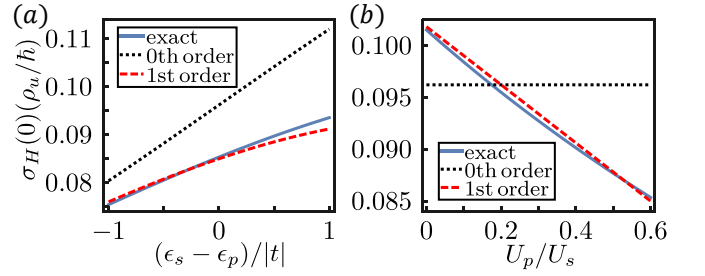


FIG. 4. Perturbative analysis of the effect of atomic interactions on the dc Hall conductivity. (a) dc Hall conductivity as a function of the orbital energy differences. Here  $\rho_u U_s = 0.7|t|$  and  $\rho_u U_p = 0.42|t|$  (b) dc Hall conductivity as a function of  $U_p/U_s$ . Here  $\epsilon_s = \epsilon_p$  and  $\rho_u U_s = 0.7|t|$ .

Eq. (13) defines the Berry curvature of the Bogoliubov bands for all momenta except for the point of  $n = 0$  and  $\mathbf{k} = \mathbf{K}$ , which has no well-defined Berry curvature [46]. Nevertheless, the quantity  $\Omega_0(\mathbf{K})$  as given by Eq. (13) is finite [47] and in fact determines the low frequency Hall conductivity of the chiral superfluid. Comparing Eq. (7) and Eq. (13) we immediately arrive at

$$\sigma_H(0) = \frac{N}{\hbar\mathcal{A}}\Omega_0(\mathbf{K}). \quad (14)$$

Even though  $\Omega_0(\mathbf{K})$  no longer has the interpretation of the Berry curvature of the Bogoliubov band, its existence has the origin in the Berry curvature of the non-interacting band. Namely we find that  $\Omega_0(\mathbf{K}) = \Omega_0^{(0)}(\mathbf{K}) + O(U_s, U_p)$  in the limit of small atomic interactions, where  $\Omega_0^{(0)}(\mathbf{K})$  is the corresponding Berry curvature of the bottom non-interacting band at  $\mathbf{K}$ . The correction due to atomic interactions can be obtained perturbatively in terms of the scattering length, although the general expression is too unwieldy and is thus relegated to the Supplemental Material [41]. For experimentally relevant parameters this correction is significant and is well captured by a first order calculation, as shown in Fig. 4(a) for a fixed scattering length. Such an agreement is also found for a range of different on-site interaction strengths. This is best illustrated by the case of  $\epsilon_s = \epsilon_p$ , for which the first order result is particularly simple and is given by

$$\sigma_H(0) = \frac{N}{\hbar\mathcal{A}} \left[ \Omega_0^{(0)}(\mathbf{K}) - \frac{\rho_u a^2}{144|t|} (5U_p - U_s) \right]. \quad (15)$$

As shown in Fig. 4(b), this result again provides an excellent account for the interaction induced correction of the dc Hall conductivity.

*Experimental proposals.*— Since atoms are charge neutral, transport properties of quantum gases cannot be measured with conventional condensed matter probes. We now outline some relevant probes designed specifically for quantum gases and can be used to detect the

anomalous Hall effect. The finite-frequency Hall response can be detected by taking advantage of the fact that quantum gases are often trapped by an additional weak harmonic potential with frequency  $\omega_{tr}$ . A periodic displacement of the trapping potential along the  $x$ -direction at frequency  $\omega$  and amplitude  $d_x$  generates a force on the atoms that mimics the effect of an electric field on electrons. The resulting center of mass motion of the gas along the  $y$ -direction can be measured by a quantum gas microscope [48] as  $R_y(\omega) \cos[\omega t - \phi_y(\omega)]$ . The Hall conductivity can then be read out as  $\sigma_H(\omega) = \text{Im}[(2N\omega/iAm\omega_{tr}^2 d_x)R_y(\omega)e^{i\phi_y(\omega)}]$  [49], where  $m$  is the mass of the atom. Such a probe has already been successfully implemented to measure the longitudinal conductivity for a Fermi gas in optical lattice [50]. However, this method is only suitable for measuring responses at frequency  $\omega > \omega_{tr}$  and thus cannot access the dc conductivity. For the latter we can resort to the so-called dichroism probe [51–53]. More specifically, one considers a circular drive of the form  $V_{\pm}(\mathbf{r}) = 2\mathcal{E}(x \cos \bar{\omega}t \pm y \sin \bar{\omega}t)$ , which induces a certain excitation rate  $\Gamma_{\pm}(\bar{\omega})$  out of the ground state. The observable of interest is provided by the differential integrated rate  $\Delta\Gamma = \frac{1}{2} \int_0^{\infty} d\bar{\omega} [\Gamma_+(\bar{\omega}) - \Gamma_-(\bar{\omega})]$ , which is related to the dc Hall conductivity via  $\sigma_H(0) = \Delta\Gamma/(2\pi\mathcal{A}\mathcal{E}^2)$  [51]. This probe has also been successfully applied to measure the Chern number in a cold atomic realization of the Haldane model [52].

*Conclusions.*—In summary, we have shown the existence of Hall responses in a recently realized bosonic chiral superfluid at zero temperature, in the absence of any artificial magnetic field or rotation of the trapping potential. The causes for such an anomalous Hall effect have been analyzed in both the low and high frequency limits. We found that the chirality of the system dictates the behavior of the high frequency response while finite Berry curvatures of the non-interacting bands underpin the dc Hall response. We point out experimental methods, already available and tested in other quantum gas systems, that can be used to detect this anomalous Hall effect. Our findings are of immediate experimental interests and may spur further studies on bosonic topological matters.

*Acknowledgement.* We are grateful to Georg Bruun and Georg Engelhardt for valuable discussions and for proof reading the manuscript. This work is supported by NSFC (Grant No. 11974161 and Grant No. U1801661), Shenzhen Science and Technology Program (Grant No. KQTD20200820113010023), the Key-Area Research and Development Program of Guangdong Province (Grant No. 2019B030330001), the National Key R&D Program of China (Grant No. 2018YFA0307200), and a grant from Guangdong province (Grant No. 2019ZT08X324).

\* xuzf@sustech.edu.cn

† wuzg@sustech.edu.cn

- [1] I. Bloch, J. Dalibard, and S. Nascimbène, *Nature Physics* **8**, 267 (2012).
- [2] I. M. Georgescu, S. Ashhab, and F. Nori, *Rev. Mod. Phys.* **86**, 153 (2014).
- [3] H. Zhai, *Ultracold Atomic Physics* (Cambridge University Press, 2021).
- [4] D. Jaksch, C. Bruder, J. I. Cirac, C. W. Gardiner, and P. Zoller, *Phys. Rev. Lett.* **81**, 3108 (1998).
- [5] I. Bloch, J. Dalibard, and W. Zwerger, *Rev. Mod. Phys.* **80**, 885 (2008).
- [6] Y. J. Lin, K. Jiménez-García, and I. B. Spielman, *Nature* **471**, 83 (2011).
- [7] V. Galitski and I. B. Spielman, *Nature* **494**, 49 (2013).
- [8] H. Zhai, *Reports on Progress in Physics* **78**, 026001 (2015).
- [9] J. Dalibard, F. Gerbier, G. Juzeliūnas, and P. Öhberg, *Rev. Mod. Phys.* **83**, 1523 (2011).
- [10] L. J. LeBlanc, K. Jiménez-García, R. A. Williams, M. C. Beeler, A. R. Perry, W. D. Phillips, and I. B. Spielman, *Proceedings of the National Academy of Sciences* **109**, 10811 (2012).
- [11] Y. Tokura and N. Nagaosa, *Science* **288**, 462 (2000).
- [12] T. Kock, C. Hippler, A. Ewerbeck, and A. Hemmerich, *Journal of Physics B: Atomic, Molecular and Optical Physics* **49**, 042001 (2016).
- [13] X. Li and W. V. Liu, *Reports on Progress in Physics* **79**, 116401 (2016).
- [14] T. Müller, S. Fölling, A. Widera, and I. Bloch, *Phys. Rev. Lett.* **99**, 200405 (2007).
- [15] G. Wirth, M. Ölschläger, and A. Hemmerich, *Nature Physics* **7**, 147 (2011).
- [16] P. Soltan-Panahi, D.-S. Lühmann, J. Struck, P. Windpassinger, and K. Sengstock, *Nature Physics* **8**, 71 (2012).
- [17] M. Ölschläger, T. Kock, G. Wirth, A. Ewerbeck, C. M. Smith, and A. Hemmerich, *New Journal of Physics* **15**, 083041 (2013).
- [18] T. Kock, M. Ölschläger, A. Ewerbeck, W.-M. Huang, L. Mathey, and A. Hemmerich, *Phys. Rev. Lett.* **114**, 115301 (2015).
- [19] M. Weinberg, C. Staarmann, C. Ölschläger, J. Simonet, and K. Sengstock, *2D Materials* **3**, 024005 (2016).
- [20] M. Hachmann, Y. Kiefer, J. Riebesehl, R. Eichberger, and A. Hemmerich, *Phys. Rev. Lett.* **127**, 033201 (2021).
- [21] J. Vargas, M. Nuske, R. Eichberger, C. Hippler, L. Mathey, and A. Hemmerich, *Phys. Rev. Lett.* **126**, 200402 (2021).
- [22] S. Jin, W. Zhang, X. Guo, X. Chen, X. Zhou, and X. Li, *Phys. Rev. Lett.* **126**, 035301 (2021).
- [23] X.-Q. Wang, G.-Q. Luo, J.-Y. Liu, W. V. Liu, A. Hemmerich, and Z.-F. Xu, *Nature* **596**, 227 (2021).
- [24] P. M. Walmsley and A. I. Golov, *Phys. Rev. Lett.* **109**, 215301 (2012).
- [25] H. Ikegami, Y. Tsutsumi, and K. Kono, *Science* **341**, 59 (2013).
- [26] B. A. Bernevig and T. L. Hughes, *Topological Insulators and Topological Superconductors* (Princeton University Press, Princeton, NJ, 2013).
- [27] D. J. Thouless, M. Kohmoto, M. P. Nightingale, and M. den Nijs, *Phys. Rev. Lett.* **49**, 405 (1982).

- [28] F. D. M. Haldane, *Phys. Rev. Lett.* **61**, 2015 (1988).
- [29] C.-X. Liu, S.-C. Zhang, and X.-L. Qi, *Annual Review of Condensed Matter Physics* **7**, 301 (2016).
- [30] N. Nagaosa, J. Sinova, S. Onoda, A. H. MacDonald, and N. P. Ong, *Rev. Mod. Phys.* **82**, 1539 (2010).
- [31] D. Xiao, M.-C. Chang, and Q. Niu, *Rev. Mod. Phys.* **82**, 1959 (2010).
- [32] A. M. Dudarev, R. B. Diener, I. Carusotto, and Q. Niu, *Phys. Rev. Lett.* **92**, 153005 (2004).
- [33] Y. Li, P. Sengupta, G. G. Batrouni, C. Miniatura, and B. Grémaud, *Phys. Rev. A* **92**, 043605 (2015).
- [34] E. van der Bijl and R. A. Duine, *Phys. Rev. Lett.* **107**, 195302 (2011).
- [35] K. Patucha, B. Grygiel, and T. A. Zaleski, *Phys. Rev. B* **97**, 214522 (2018).
- [36] E. Taylor and C. Kallin, *Phys. Rev. Lett.* **108**, 157001 (2012).
- [37] R. M. Lutchyn, P. Nagornykh, and V. M. Yakovenko, *Phys. Rev. B* **80**, 104508 (2009).
- [38] C. Kallin and J. Berlinsky, *Reports on Progress in Physics* **79**, 054502 (2016).
- [39] P. M. R. Brydon, D. S. L. Abergel, D. F. Agterberg, and V. M. Yakovenko, *Phys. Rev. X* **9**, 031025 (2019).
- [40] M. D. E. Denys and P. M. R. Brydon, *Phys. Rev. B* **103**, 094503 (2021).
- [41] Supplemental Material.
- [42] Z. Zhou, L.-L. Wan, and Z.-F. Xu, *Journal of Physics A: Mathematical and Theoretical* **53**, 425203 (2020).
- [43] B. S. Shastry, B. I. Shraiman, and R. R. P. Singh, *Phys. Rev. Lett.* **70**, 2004 (1993).
- [44] R. Shindou, R. Matsumoto, S. Murakami, and J.-i. Ohe, *Phys. Rev. B* **87**, 174427 (2013).
- [45] G. Engelhardt and T. Brandes, *Phys. Rev. A* **91**, 053621 (2015).
- [46] S. Furukawa and M. Ueda, *New Journal of Physics* **17**, 115014 (2015).
- [47] We note that in the expression for  $\Omega_0(\mathbf{K})$  the summation over the band index excludes  $\bar{0}$  since  $n = 0, \mathbf{k} = \mathbf{K}$  and  $n = \bar{0}, \mathbf{k} = \mathbf{K}$  refer to the same ground state.
- [48] S. Kuhr, *National Science Review* **3**, 170 (2016).
- [49] Z. Wu, E. Taylor, and E. Zaremba, *EPL (Europhysics Letters)* **110**, 26002 (2015).
- [50] R. Anderson, F. Wang, P. Xu, V. Venu, S. Trotzky, F. Chevy, and J. H. Thywissen, *Phys. Rev. Lett.* **122**, 153602 (2019).
- [51] D. T. Tran, A. Dauphin, A. G. Grushin, P. Zoller, and N. Goldman, *Science Advances* **3**, 1701207 (2017).
- [52] L. Asteria, D. T. Tran, T. Ozawa, M. Tarnowski, B. S. Rem, N. Fläschner, K. Sengstock, N. Goldman, and C. Weitenberg, *Nature Physics* **15**, 449 (2019).
- [53] J. M. Midtgaard, Z. Wu, N. Goldman, and G. M. Bruun, *Phys. Rev. Research* **2**, 033385 (2020).

## Supplementary Material for “Intrinsic Anomalous Hall Effect in a Bosonic Chiral Superfluid”

This supplemental material contains the following five sections: (I) Derivation of the multi-orbital Bose-Hubbard model; (II) Determination of the superfluid ground state; (III) Symmetry properties of the  $\mathbf{K}$  and  $\mathbf{K}'$  points; (IV) Loop currents; and (V) Perturbative treatment of the Hall conductivity.

### DERIVATION OF THE MULTI-ORBITAL BOSE-HUBBARD MODEL

In this section we provide the derivation of the multi-orbital Bose-Hubbard model used to describe the experimental system. The ultracold  $^{87}\text{Rb}$  gas is confined in a 2D boron nitride (BN) optical lattice potential formed by the superimposition of two sets of triangular lattice potentials with different depths [1], i.e.,

$$V_{\text{BN}}(\mathbf{x}) = - \sum_{\beta=1,2} V_{\beta} \left\{ 3 + 2 \sum_{\langle i,j \rangle} \cos \left[ (\mathbf{k}_i - \mathbf{k}_j) \cdot \mathbf{x} + (-1)^{\beta} \frac{2\pi}{3} \right] \right\}, \quad (\text{S1})$$

where the summation  $\langle i, j \rangle$  is restricted to  $\langle 1, 2 \rangle$ ,  $\langle 2, 3 \rangle$  and  $\langle 3, 1 \rangle$ , and  $\mathbf{k}_1 = k_L(-\sqrt{3}/2, 1/2)$ ,  $\mathbf{k}_2 = k_L(\sqrt{3}/2, 1/2)$ , and  $\mathbf{k}_3 = k_L(0, -1)$  are wavevectors of three laser beams intersecting at  $120^\circ$  angle. Here we use  $\mathbf{x} = (x, y)$  to denote the continuous 2D coordinate, to be distinguished from the discrete vector  $\mathbf{r}$  used to denote the lattice sites. The profile of such a potential for  $V_1 \neq V_2$  is shown in Fig. S1(a); the local minima of  $V_{\text{BN}}(\mathbf{x})$ , denoted by  $\mathbf{r}$ , form a hexagonal lattice spanned by primitive vectors  $\mathbf{a}_1 = a(\sqrt{3}/2, -1/2)$  and  $\mathbf{a}_2 = a(\sqrt{3}/2, 1/2)$ , where  $a = 4\pi/3k_L$  is the lattice constant. The two sublattices of the hexagonal lattice are denoted by  $A$  and  $B$  respectively.

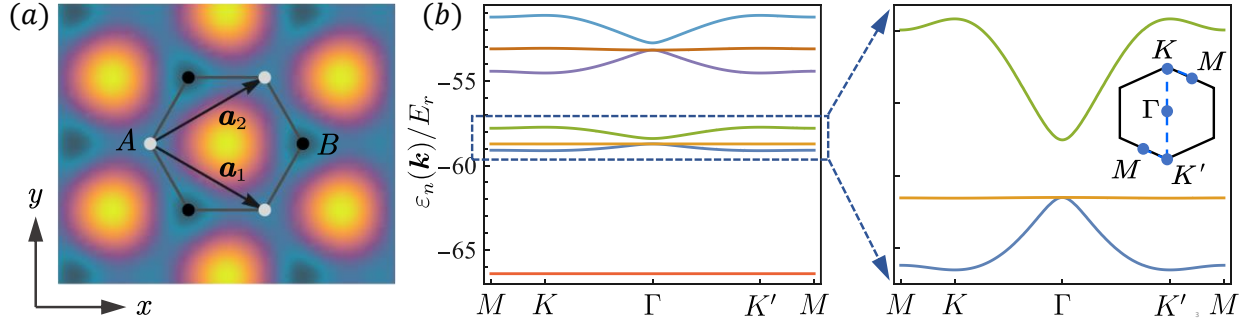


FIG. S1. Here the potential depths are  $V_1 = 7.23E_r$ ,  $V_2 = 8.35E_r$ , where  $E_r = \frac{\hbar^2 k_L^2}{2m}$  is the recoil energy. (a) The profile of the lattice potential and the Wigner-Seitz cell. (b) The lowest several bands of Hamiltonian  $H_0$  along the high-symmetry points in the first Brillouin zone.

The potential depths  $V_1$  and  $V_2$  in  $V_{\text{BN}}(\mathbf{x})$  can be arbitrarily tuned and the corresponding band structure easily calculated numerically. We consider an experimentally relevant parameter region where the local  $s$ -orbital on one set of sublattice sites (say  $A$ ) and the local  $p$ -orbitals on the other (say  $B$ ) have comparable energies. In such a case, the second, third and fourth bands are isolated from the rest in energy and form a subspace in which an effective Hamiltonian for the system of interest can be constructed (see Fig. S1 (b) and Fig. S2 (a)).

To proceed, we first construct the so-called maximally localized Wannier functions from the numerically calculated Bloch states of these three bands [2], which describe the local orbitals on the lattice sites. We thus obtain three Wannier functions  $w_{s,\mathbf{r}}(\mathbf{x})$  and  $w_{p,\mathbf{r}}^\alpha(\mathbf{x})$  ( $\alpha = \pm$ ). The  $s$ -orbital function  $w_{s,\mathbf{r}}(\mathbf{x})$  centers at lattice vector  $\mathbf{r} \in A$  and can be chosen as real; the two  $p$ -orbital functions  $w_{p,\mathbf{r}}^\alpha$  centers at lattice vector  $\mathbf{r} \in B$  and are time-reversed counterparts of each other.

For experimentally relevant parameters, the dispersions of the three bands of interest can be reproduced accurately by the following tight-binding model

$$\hat{H}_0 = \sum_{\mathbf{r} \in A} \epsilon_s \hat{s}_{\mathbf{r}}^\dagger \hat{s}_{\mathbf{r}} + \sum_{\mathbf{r} \in B, \alpha} \epsilon_p \hat{p}_{\alpha, \mathbf{r}}^\dagger \hat{p}_{\alpha, \mathbf{r}} + \sum_{\mathbf{r} \in A, l, \alpha} (t_l^\alpha \hat{s}_{\mathbf{r}}^\dagger \hat{p}_{\alpha, \mathbf{r} + \delta_l} + h.c.), \quad (\text{S2})$$

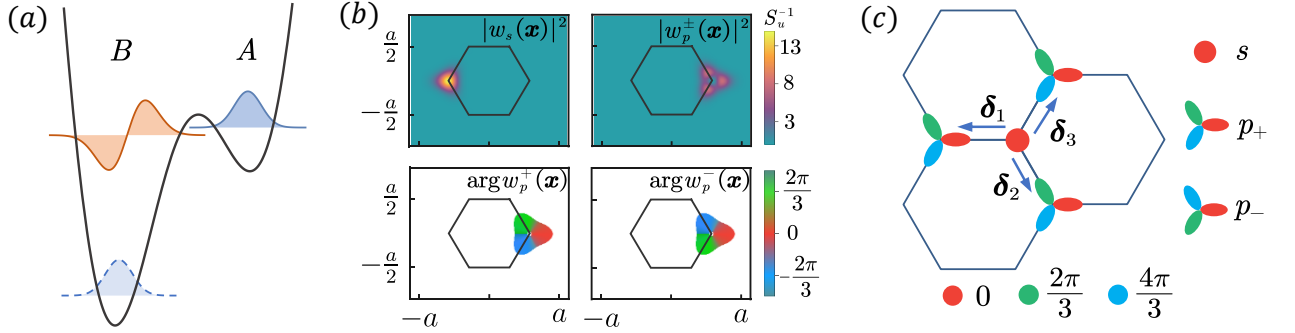


FIG. S2. (a) Schematic illustration of local orbitals. The on-site energy of the  $s$ -orbital on A site is comparable to that of the  $p$ -orbitals on B site. (b) Amplitudes and phases of the calculated Wannier functions. Here  $S_u = \frac{\sqrt{3}}{2}a^2$  is the area of the unit cell. (c) The hopping of atoms between the  $s$ -orbital on A site and  $p$ -orbital on the nearest-neighbor sites. The red, green and blue color represents the phase winding of 0,  $2\pi/3$  and  $4\pi/3$  respectively.

where  $\hat{s}_r$  and  $\hat{p}_{\alpha,r}$  are annihilation operators for the Wannier orbitals  $w_{s,r}$  and  $w_{p,\alpha,r}^\alpha$  respectively, and  $\delta_l = \frac{a}{\sqrt{3}}(\cos \frac{2l+1}{3}\pi, \sin \frac{2l+1}{3}\pi)$ ,  $l = 1, 2, 3$  (see Fig. S2). The on-site energies  $\epsilon_s$  and  $\epsilon_p$ , and the hopping matrix element  $t_l^\alpha$  between the  $s$  orbital and the nearest-neighbor  $p_\alpha$  orbitals are determined by

$$\begin{aligned}\epsilon_s &= \int w_{s,r}^*(\mathbf{x}) \left[ \frac{-\hbar^2 \nabla^2}{2m} + V_{\text{BN}}(\mathbf{x}) \right] w_{s,r}(\mathbf{x}) d\mathbf{x} \\ \epsilon_p &= \int w_{p,r}^{\alpha*}(\mathbf{x}) \left[ \frac{-\hbar^2 \nabla^2}{2m} + V_{\text{BN}}(\mathbf{x}) \right] w_{p,r}^\alpha(\mathbf{x}) d\mathbf{x} \\ t_l^\alpha &= \int w_{s,r}^*(\mathbf{x}) \left[ \frac{-\hbar^2 \nabla^2}{2m} + V_{\text{BN}}(\mathbf{x}) \right] w_{p,r+\delta_l}^\alpha(\mathbf{x}) d\mathbf{x}.\end{aligned}\quad (\text{S3})$$

Since the Hamiltonian preserves the  $D_3$  point-group symmetry, the maximally localized Wannier functions are the basis functions of irreducible representations of  $D_3$  group. Indeed, if we define operations  $\mathcal{R}, \mathcal{S} \in D_3$ , where  $\mathcal{R}$  is the counterclockwise rotation of  $2\pi/3$  around the  $z$  axis and  $\mathcal{S}$  is the reflection across the  $x$  axis, we have

$$\begin{aligned}\mathcal{S}w_{s,r}(\mathbf{x}) &= w_{s,r}(\mathbf{x}); & \mathcal{S}w_{p,r}^+(\mathbf{x}) &= w_{p,r}^-(\mathbf{x}) \\ \mathcal{R}w_{s,r}(\mathbf{x}) &= w_{s,r}(\mathbf{x}); & \mathcal{R}w_{p,r}^\alpha(\mathbf{x}) &= e^{-i\alpha 2\pi/3} w_{p,r}^\alpha(\mathbf{x}).\end{aligned}\quad (\text{S4})$$

Such properties are reflected in Fig S2 (b) in which the calculated Wannier functions are plotted. Using these properties it's straightforward to show that

$$t_l^+ = (t_l^-)^* = t e^{i(l-1)2\pi/3}, \quad (\text{S5})$$

where  $t \in \mathbb{R}$ .

Finally, as a result of angular momentum conservation, the interactions between the atoms can be described by the Hamiltonian

$$\hat{H}_{\text{int}} = \frac{U_s}{2} \sum_{\mathbf{r} \in A} \hat{s}_r^\dagger \hat{s}_r^\dagger \hat{s}_r \hat{s}_r + \frac{U_p}{2} \sum_{\mathbf{r} \in B} \left( \sum_{\alpha} \hat{p}_{\alpha,r}^\dagger \hat{p}_{\alpha,r}^\dagger \hat{p}_{\alpha,r} \hat{p}_{\alpha,r} + 4\hat{p}_{+,r}^\dagger \hat{p}_{-,r}^\dagger \hat{p}_{-,r} \hat{p}_{+,r} \right). \quad (\text{S6})$$

The on-site interaction strengths are given by

$$U_s = \frac{4\pi\hbar^2 a_s}{m} \int d\mathbf{x} |w_{s,r}(\mathbf{x})|^4; \quad U_p = \frac{4\pi\hbar^2 a_s}{m} \int d\mathbf{x} |w_{p,r}^+(\mathbf{x})|^4, \quad (\text{S7})$$

where  $a_s$  is the effective scattering length of the quasi-2D system.



## DETERMINATION OF THE SUPERFLUID GROUND STATE

In this section we provide more details on the determination of the mean-field ground state, which is best carried out in momentum space. In momentum space the non-interacting Hamiltonian can be written as

$$\hat{H}_0 = \sum_{\mathbf{k}} \hat{\psi}_{\mathbf{k}}^\dagger h_0(\mathbf{k}) \hat{\psi}_{\mathbf{k}}, \quad (\text{S8})$$

where  $\hat{\psi}_{\mathbf{k}} = (\hat{s}_{\mathbf{k}} \hat{p}_{+, \mathbf{k}} \hat{p}_{-, \mathbf{k}})^T$  and

$$h_0(\mathbf{k}) = \begin{pmatrix} \epsilon_s & f_{\mathbf{k}}^+ & f_{\mathbf{k}}^- \\ & \epsilon_p & 0 \\ h.c. & & \epsilon_p \end{pmatrix} \quad (\text{S9})$$

with  $f_{\mathbf{k}}^\alpha = \sum_l t_l^\alpha e^{i\mathbf{k} \cdot \delta_l}$ . Here the operators in momentum space are defined as the discrete Fourier transform of those in real space, e.g.,  $\hat{s}_{\mathbf{k}} = \frac{1}{\sqrt{N_u}} \sum_{\mathbf{r} \in A} e^{-i\mathbf{k} \cdot \mathbf{r}} \hat{s}_{\mathbf{r}}$ . The non-interacting band structure is given by the eigenvalues of  $h_0(\mathbf{k})$

$$\epsilon_0(\mathbf{k}) = \frac{1}{2} [\epsilon_s + \epsilon_p - \sqrt{(\epsilon_s - \epsilon_p)^2 + 4(|f_{\mathbf{k}}^+|^2 + |f_{\mathbf{k}}^-|^2)}]; \quad (\text{S10})$$

$$\epsilon_1(\mathbf{k}) = \epsilon_p; \quad (\text{S11})$$

$$\epsilon_2(\mathbf{k}) = \frac{1}{2} [\epsilon_s + \epsilon_p + \sqrt{(\epsilon_s - \epsilon_p)^2 + 4(|f_{\mathbf{k}}^+|^2 + |f_{\mathbf{k}}^-|^2)}]. \quad (\text{S12})$$

Since the local minima of the bottom band occur at  $\mathbf{K}$  and  $\mathbf{K}'$ , we can assume that the condensate wave function is the superposition of single-particle wave functions at these momentum and express the trial solution in real space as

$$\begin{aligned} \langle \hat{s}_{\mathbf{r}} \rangle &= \sqrt{\rho_u} \left( e^{i\mathbf{K} \cdot \mathbf{r}} \varphi_{s, \mathbf{K}} + e^{i\mathbf{K}' \cdot \mathbf{r}} \varphi_{s, \mathbf{K}'} \right) \\ \langle \hat{p}_{\alpha, \mathbf{r}} \rangle &= \sqrt{\rho_u} \left( e^{i\mathbf{K} \cdot \mathbf{r}} \varphi_{p, \mathbf{K}}^\alpha + e^{i\mathbf{K}' \cdot \mathbf{r}} \varphi_{p, \mathbf{K}'}^\alpha \right), \end{aligned} \quad (\text{S13})$$

where  $\rho_u$  is the number of atoms per unit cell, and the variables at  $\mathbf{K}$  and  $\mathbf{K}'$  are independent. Using Eq. (S13) in Eq. (S2) and Eq. (S6), we obtain the kinetic energy functional

$$E_0 = N \left[ \Phi_{\mathbf{K}}^\dagger h_0(\mathbf{K}) \Phi_{\mathbf{K}} + \Phi_{\mathbf{K}'}^\dagger h_0(\mathbf{K}') \Phi_{\mathbf{K}'} \right] \quad (\text{S14})$$

where  $\Phi_{\mathbf{K}(\mathbf{K}')} = \left( \varphi_{s, \mathbf{K}(\mathbf{K}')} , \varphi_{p, \mathbf{K}(\mathbf{K}')}^+ , \varphi_{p, \mathbf{K}(\mathbf{K}')}^- \right)^T$ , and the interaction energy functional

$$\begin{aligned} E_{\text{int}} &= N \left[ \frac{\rho_u U_s}{2} (|\varphi_{s, \mathbf{K}}|^4 + |\varphi_{s, \mathbf{K}'}|^4 + 4|\varphi_{s, \mathbf{K}}|^2 |\varphi_{s, \mathbf{K}'}|^2) \right. \\ &\quad + \sum_{\alpha} \frac{\rho_u U_p}{2} (|\varphi_{p, \mathbf{K}}^\alpha|^4 + |\varphi_{p, \mathbf{K}'}^\alpha|^4 + 4|\varphi_{p, \mathbf{K}}^\alpha|^2 |\varphi_{p, \mathbf{K}'}^\alpha|^2) \\ &\quad \left. + 2\rho_u U_p \left( |\varphi_{p, \mathbf{K}}^+ \varphi_{p, \mathbf{K}}^-|^2 + |\varphi_{p, \mathbf{K}'}^+ \varphi_{p, \mathbf{K}'}^-|^2 + |\varphi_{p, \mathbf{K}}^+ \varphi_{p, \mathbf{K}'}^- + \varphi_{p, \mathbf{K}'}^+ \varphi_{p, \mathbf{K}}^-|^2 \right) \right]. \end{aligned} \quad (\text{S15})$$

The ground state can be determined by minimizing the Gross-Pitaevskii energy functional  $E_0 + E_{\text{int}}$  under the constraint  $(|\varphi_{s, \mathbf{K}}|^2 + |\varphi_{s, \mathbf{K}'}|^2) + \sum_{\alpha} (|\varphi_{p, \mathbf{K}}^\alpha|^2 + |\varphi_{p, \mathbf{K}'}^\alpha|^2) = 1$ . We find that the solutions corresponding to either  $\mathbf{K}$  or  $\mathbf{K}'$  condensation have the lowest energy, i.e., the time-reversal symmetry is spontaneously broken in the ground state. More specifically, we find that the mean-field ground state in momentum space takes the form of

$$\langle \hat{\psi}_{\mathbf{k}} \rangle = \sqrt{N} (\cos \xi \sin \xi \ 0)^T \delta_{\mathbf{k}, \mathbf{K}}, \quad \text{or} \quad \langle \hat{\psi}_{\mathbf{k}} \rangle = \sqrt{N} (\cos \xi \ 0 \ \sin \xi)^T \delta_{\mathbf{k}, \mathbf{K}'}. \quad (\text{S16})$$

An example of the condensate wave function in real space is shown in Fig. S3 (a) and (b). The time-reversal symmetry breaking can be corroborated by the fact that any superposition of the above two wave functions no longer preserves the  $C_3$  symmetry (see the symmetry group analysis in Sec. ), as illustrated in Fig. S3 (c).

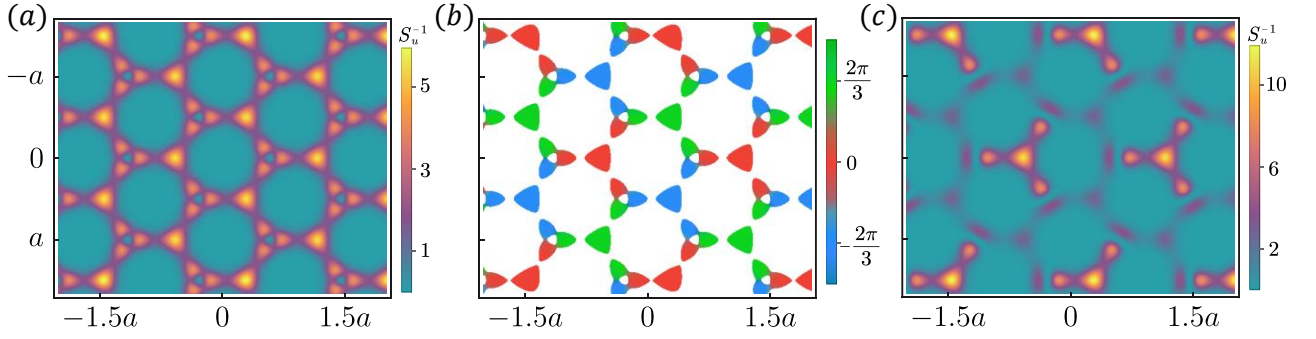


FIG. S3. The parameters for the calculations shown are  $\epsilon_s - \epsilon_p = 0.5|t|$ ,  $\rho_u U_s = 1.2|t|$  and  $\rho_u U_p = 0.72|t|$ . Here  $S_u = \frac{\sqrt{3}}{2}a^2$  is the area of the unit cell. (a) Ground state density distribution corresponding to the condensate wave function  $\langle \hat{\psi}_{\mathbf{k}} \rangle = \sqrt{N}(\cos \xi \ \sin \xi \ 0)^T \delta_{\mathbf{k}, \mathbf{K}}$ , where  $\cos \xi = 0.67$ . (b) The phase of the condensate wave function in real space. (c) Density distribution corresponding to an equal weight superposition of both  $\mathbf{K}$  and  $\mathbf{K}'$  condensate wave functions.

### SYMMETRY PROPERTIES OF THE $\mathbf{K}$ AND $\mathbf{K}'$ POINTS

In this section, we demonstrate, by means of symmetry group analysis, two effects that are direct consequences of the symmetrical properties of the  $\mathbf{K}$  and  $\mathbf{K}'$  points: (a) in real space the atoms on  $B$  sites are all in  $p_+$  ( $p_-$ )-orbitals when the atoms condense at  $\mathbf{K}$  ( $\mathbf{K}'$ ) point in momentum space, i.e., the correlation between the chirality and the momentum condensation; and (b) the current operator does not couple the ground state to the excitation at  $\mathbf{K}$  in the second Bogoliubov band, i.e., the current operator selection rule. By virtue of the symmetry analysis, the validity of these result is quite general and is not contingent on the validity of the tight-binding model.

By the symmetrical properties of the  $\mathbf{K}$  and  $\mathbf{K}'$  points we mean that the Bloch states at these points can be classified according to the irreducible representations of the  $C_3$  group. Since the Bloch states are related to the Wannier states by  $\phi_{s, \mathbf{k}}(\mathbf{x}) = \frac{1}{\sqrt{N_u}} \sum_{\mathbf{r} \in A} e^{i\mathbf{k} \cdot \mathbf{r}} w_{s, \mathbf{r}}(\mathbf{x})$ , it is straightforward to check that these states at  $\mathbf{K}$  and  $\mathbf{K}'$  transform as follows under the rotation of  $2\pi/3$

$$\begin{aligned} \mathcal{R}\phi_{s, \mathbf{K}}(\mathbf{x}) &= e^{-i\frac{2\pi}{3}} \phi_{s, \mathbf{K}}(\mathbf{x}), & \mathcal{R}\phi_{p, \mathbf{K}}^\alpha(\mathbf{x}) &= e^{-i\alpha\frac{2\pi}{3}} \phi_{p, \mathbf{K}}^\alpha(\mathbf{x}); \\ \mathcal{R}\phi_{s, \mathbf{K}'}(\mathbf{x}) &= e^{i\frac{2\pi}{3}} \phi_{s, \mathbf{K}'}(\mathbf{x}), & \mathcal{R}\phi_{p, \mathbf{K}'}^\alpha(\mathbf{x}) &= e^{-i\alpha\frac{2\pi}{3}} \phi_{p, \mathbf{K}'}^\alpha(\mathbf{x}). \end{aligned} \quad (\text{S17})$$

Thus these six functions can be divided into two sets, each consisting of three basis functions of an irreducible representation of the  $C_3$  group (see Tab. S1).

$C_3$	$\mathcal{I}$	$\mathcal{R}$	$\mathcal{R}^2$	basis functions		
$A_2$	1	$e^{-i2\pi/3}$	$e^{-i4\pi/3}$	$\phi_{s, \mathbf{K}}$	$\phi_{p, \mathbf{K}}^+$	$\phi_{p, \mathbf{K}'}^+$
$A_3$	1	$e^{i2\pi/3}$	$e^{i4\pi/3}$	$\phi_{s, \mathbf{K}'}$	$\phi_{p, \mathbf{K}}^-$	$\phi_{p, \mathbf{K}'}^-$

TABLE S1. Character table of non-identity irreducible representations of the  $C_3$  group.

Now, if the condensate wave function preserves the  $C_3$  symmetry, it must be a superposition of basis functions belonging to a specific irreducible representation of  $C_3$ . If we assume that the atoms condense at  $\mathbf{K}$ , we immediately see from the character table that the condensate wave function must either be a superposition of  $\phi_{s, \mathbf{K}}$  and  $\phi_{p, \mathbf{K}}^+$  (belonging to  $A_2$ ), or be proportional to  $\phi_{p, \mathbf{K}}^-$  (belonging to  $A_3$ ). For the superfluid state it's clearly the former since the non-interacting ground state at  $\mathbf{K}$  is a mixture of the  $s$  and  $p_+$  orbitals. This proves that the condensation at  $\mathbf{K}$  in momentum space implies the condensation in the  $p_+$  orbitals on the  $B$  sublattice in real space. The case of condensation at  $\mathbf{K}'$  can be similarly analyzed.

To show the selection rule of the current operator, we consider the following three states: the ground state, denoted by  $|E_0(\mathbf{K})\rangle$ , the state containing a momentum  $\mathbf{K}$  excitation of the first Bogoliubov band, denoted by  $|E_1(\mathbf{K})\rangle$  and the state containing a momentum  $\mathbf{K}$  excitation of the second Bogoliubov band, denoted by  $|E_2(\mathbf{K})\rangle$ . From the  $C_3$  symmetry analysis we again find that  $|E_0(\mathbf{K})\rangle$  and  $|E_2(\mathbf{K})\rangle$  belong to the  $A_2$  representation while  $|E_1(\mathbf{K})\rangle$  belongs

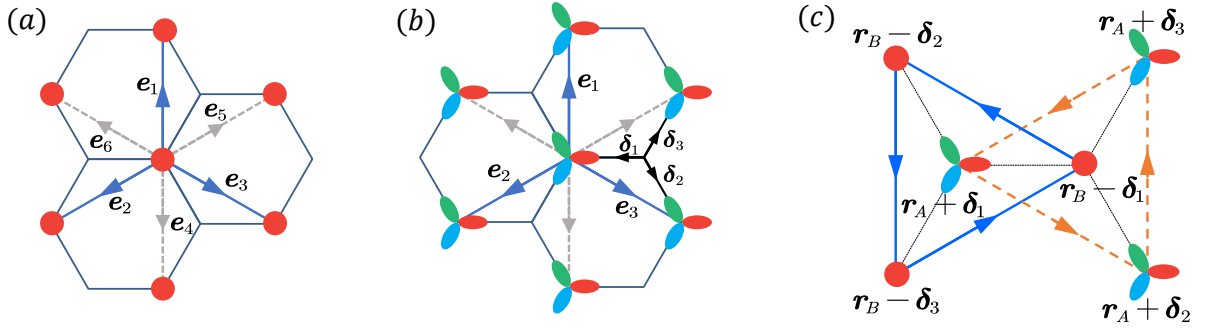


FIG. S4. (a) Schematic illustration of NNN hoppings between  $s$  orbitals. (b) Illustration of NNN hoppings between the  $p_+$  orbitals (c) Illustration of the loop currents along the closed paths passing through three nearest-neighbor  $s$  orbitals and three nearest-neighbor  $p_+$  orbitals.

to the  $A_3$ . Furthermore, we note that under the rotation  $\mathcal{R}$  the current operator transforms as

$$\mathcal{R} \begin{pmatrix} \hat{J}_x \\ \hat{J}_y \end{pmatrix} \mathcal{R}^{-1} = \begin{pmatrix} \cos \frac{2\pi}{3} & -\sin \frac{2\pi}{3} \\ \sin \frac{2\pi}{3} & \cos \frac{2\pi}{3} \end{pmatrix} \begin{pmatrix} \hat{J}_x \\ \hat{J}_y \end{pmatrix} \quad (\text{S18})$$

Defining  $\hat{J}_\alpha = (\hat{J}_x - \alpha i \hat{J}_y)/2$  ( $\alpha = \pm$ ), this means that

$$\mathcal{R} \hat{J}_\alpha \mathcal{R}^{-1} = e^{-\alpha i \frac{2\pi}{3}} \hat{J}_\alpha. \quad (\text{S19})$$

Thus we find that

$$\begin{aligned} \langle E_2(\mathbf{K}) | \hat{J}_\alpha | E_0(\mathbf{K}) \rangle &= \langle E_2(\mathbf{K}) | \mathcal{R}^\dagger \mathcal{R} \hat{J}_\alpha \mathcal{R}^\dagger \mathcal{R} | E_0(\mathbf{K}) \rangle \\ &= e^{-\alpha i \frac{2\pi}{3}} \langle E_2(\mathbf{K}) | \hat{J}_\alpha | E_0(\mathbf{K}) \rangle, \end{aligned} \quad (\text{S20})$$

which immediately leads to the aforementioned selection rule:  $\langle E_2(\mathbf{K}) | \hat{J} | E_0(\mathbf{K}) \rangle = 0$ .

## LOOP CURRENTS

In this section, we derive the expression of the loop current in terms of the loop current correlations, assuming the presence of next-nearest neighbor (NNN) hoppings (or, equivalently, nearest neighbor hoppings *within* the same sublattice). In the experimental system that we have considered in the main text, the NNN hoppings are at least an order of magnitude smaller compared to the nearest neighbor hoppings, and can thus be safely discarded. Here we include them only for the purpose of illustrating the relation between the loop current and the loop current correlations. When the NNN hoppings are taken into consideration, the Hamiltonian gains an additional term

$$\hat{H}_{\text{NNN}} = \sum_{\mathbf{k}} \hat{\psi}_{\mathbf{k}}^\dagger h_{\text{NNN}}(\mathbf{k}) \hat{\psi}_{\mathbf{k}}, \quad (\text{S21})$$

where

$$h_{\text{NNN}}(\mathbf{k}) = \begin{pmatrix} f_{\text{NNN}}^s(\mathbf{k}) & 0 & 0 \\ h.c. & f_{\text{NNN}}^{++}(\mathbf{k}) & f_{\text{NNN}}^{+-}(\mathbf{k}) \\ & & f_{\text{NNN}}^{--}(\mathbf{k}) \end{pmatrix}. \quad (\text{S22})$$

Here the matrix elements are  $f_{\text{NNN}}^s = \sum_{j=1}^6 t_{s,j} e^{i\mathbf{k}\cdot\mathbf{e}_j}$  and  $f_{\text{NNN}}^{\alpha\alpha'} = \sum_{j=1}^6 t_{p,j}^{\alpha\alpha'} e^{i\mathbf{k}\cdot\mathbf{e}_j}$ , where  $\mathbf{e}_j = (\cos \frac{4j-1}{6}\pi, \sin \frac{4j-1}{6}\pi)a$  for  $1 \leq j \leq 3$  and  $\mathbf{e}_j = -\mathbf{e}_{j-3}$  for  $4 \leq j \leq 6$  (see Fig. [S4] (a) and (b)); the hopping parameters between the nearest neighbor  $s$  orbitals are denoted by real  $t_{s,j} < 0$  and those between the nearest neighbor  $p_\alpha$  orbitals by complex  $t_{p,j}^{\alpha\alpha'}$ .

The contribution to the current operator due to the NNN hoppings is

$$\begin{aligned}\hat{\mathbf{J}}_{\text{NNN}} &= \hbar^{-1} \sum_{\mathbf{k}} \hat{\psi}_{\mathbf{k}}^{\dagger} \nabla_{\mathbf{k}} h_{\text{NNN}}(\mathbf{k}) \hat{\psi}_{\mathbf{k}} \\ &= \sum_{j=1}^3 i \mathbf{e}_j \left[ \sum_{\mathbf{r} \in A} t_{s,j} \hat{s}_{\mathbf{r}}^{\dagger} \hat{s}_{\mathbf{r}+\mathbf{e}_j} + \sum_{\mathbf{r} \in B, \alpha \alpha'} t_{p,j}^{\alpha \alpha'} \hat{p}_{\alpha, \mathbf{r}}^{\dagger} \hat{p}_{\alpha', \mathbf{r}+\mathbf{e}_j} \right] + h.c.,\end{aligned}\quad (\text{S23})$$

where only the summation over  $1 \leq j \leq 3$  is needed. Using the rotational properties of the Wannier functions, it can be shown that  $t_{s,j}$  does not depend on  $j$  and thus we can write  $t_{s,j} = -|t_s|$ ; in addition, we have  $t_{p,j}^{++} = (t_{p,j}^{--})^*$  and  $t_{p,j}^{+-} = (t_{p,j}^{-+})^*$ ; finally for  $t_{p,j}^{++}$  and  $t_{p,j}^{+-}$  where  $\mathbf{e}_j = \boldsymbol{\delta}_l - \boldsymbol{\delta}_{l'}$ , it can be shown that  $t_{p,j}^{++} = |t_p^{++}| e^{i\mathbf{K} \cdot (\boldsymbol{\delta}_l - \boldsymbol{\delta}_{l'})}$  and  $t_{p,j}^{+-} = |t_p^{+-}| e^{i\mathbf{K} \cdot (\boldsymbol{\delta}_l + \boldsymbol{\delta}_{l'})}$ . From these properties and the fact that  $\mathbf{e}_1 = \boldsymbol{\delta}_3 - \boldsymbol{\delta}_2$ ,  $\mathbf{e}_2 = \boldsymbol{\delta}_1 - \boldsymbol{\delta}_3$  and  $\mathbf{e}_3 = \boldsymbol{\delta}_2 - \boldsymbol{\delta}_1$ , the NNN current can be written as

$$\begin{aligned}\hat{\mathbf{J}}_{\text{NNN}} &= -i|t_s| \sum_{\mathbf{r} \in B, \langle ll' \rangle} \left[ (\boldsymbol{\delta}_{l'} - \boldsymbol{\delta}_l) \hat{s}_{\mathbf{r}-\boldsymbol{\delta}_{l'}}^{\dagger} \hat{s}_{\mathbf{r}-\boldsymbol{\delta}_l} - h.c. \right] \\ &\quad - i \sum_{\alpha, \alpha'} |t_p^{\alpha \alpha'}| \sum_{\mathbf{r} \in A, \langle ll' \rangle} \left[ (\boldsymbol{\delta}_{l'} - \boldsymbol{\delta}_l) e^{i\theta_{ll'}^{\alpha \alpha'}} \hat{p}_{\alpha', \mathbf{r}+\boldsymbol{\delta}_{l'}}^{\dagger} \hat{p}_{\alpha, \mathbf{r}+\boldsymbol{\delta}_l} - h.c. \right],\end{aligned}\quad (\text{S24})$$

where  $\langle ll' \rangle$  denotes the summation over the cyclic permutations (12);(23);(31). Now, loop currents in a lattice system are equivalent to integrations of current density along closed paths (loops) in the continuum space. We consider the total contribution from all those loops immediately surrounding the  $A$  and  $B$  sites, as illustrated in Fig. S4 (c), and arrive at the following loop current

$$\begin{aligned}J_{\text{loop}} &= i|t_s| \sum_{\mathbf{r} \in B, \langle ll' \rangle} \left[ |\boldsymbol{\delta}_{l'} - \boldsymbol{\delta}_l| \hat{s}_{\mathbf{r}-\boldsymbol{\delta}_{l'}}^{\dagger} \hat{s}_{\mathbf{r}-\boldsymbol{\delta}_l} - h.c. \right] \\ &\quad - i \sum_{\alpha, \alpha'} |t_p^{\alpha \alpha'}| \sum_{\mathbf{r} \in A, \langle ll' \rangle} \left[ |\boldsymbol{\delta}_{l'} - \boldsymbol{\delta}_l| e^{i\theta_{ll'}^{\alpha \alpha'}} \hat{p}_{\alpha', \mathbf{r}+\boldsymbol{\delta}_{l'}}^{\dagger} \hat{p}_{\alpha, \mathbf{r}+\boldsymbol{\delta}_l} - h.c. \right],\end{aligned}\quad (\text{S25})$$

which is nothing but

$$J_{\text{loop}} = -a(|t_s| \hat{C}_s + \sum_{\alpha \alpha'} |t_p^{\alpha \alpha'}| \hat{C}_p^{\alpha \alpha'}).\quad (\text{S26})$$

## PERTURBATIVE TREATMENT OF THE HALL CONDUCTIVITY

In this section, we provide more details on the perturbative treatment of the Hall conductivity in terms of the atomic interactions. In the dc limit, this analysis allows us to make the connection between the Hall conductivity and the Berry curvature of the non-interacting bands. Instead of starting from the formula Eq. (7) in the main text, it is more convenient to derive an alternative formula for the Hall conductivity, expressed in terms of the single-particle Green's function.

In the momentum space, the current operator is given by

$$\hat{\mathbf{J}} = \hbar^{-1} \sum_{\mathbf{k}} \hat{\psi}_{\mathbf{k}}^{\dagger} \nabla_{\mathbf{k}} h_0(\mathbf{k}) \hat{\psi}_{\mathbf{k}}.\quad (\text{S27})$$

Assuming the  $\mathbf{K}$  condensation and under the Bogoliubov approximation, this can be written as (dropping the constant term)

$$\begin{aligned}\hat{\mathbf{J}} &\approx \hbar^{-1} \left[ \hat{\psi}_{\mathbf{K}}^{\dagger} \nabla_{\mathbf{K}} h_0(\mathbf{K}) \langle \hat{\psi}_{\mathbf{K}} \rangle + \langle \hat{\psi}_{\mathbf{K}}^{\dagger} \rangle \nabla_{\mathbf{K}} h_0(\mathbf{K}) \hat{\psi}_{\mathbf{K}} \right] \\ &= \hbar^{-1} \mathcal{J}^{\dagger} \hat{\Psi}_{\mathbf{K}},\end{aligned}\quad (\text{S28})$$

where

$$\mathcal{J} \equiv \nabla_{\mathbf{k}} \mathcal{H}_B(\mathbf{K}) \tau_z \langle \hat{\Psi}_{\mathbf{K}} \rangle\quad (\text{S29})$$

and  $\hat{\Psi}_{\mathbf{k}} \equiv (\hat{\psi}_{\mathbf{k}}^T, \hat{\psi}_{2\mathbf{K}-\mathbf{k}}^\dagger)^T$ . Using Eq. (S28) in Eq. (3) of the main text and noting that  $\mathcal{J}^\dagger \hat{\Psi}_{\mathbf{K}} = \hat{\Psi}_{\mathbf{K}}^\dagger \mathcal{J}$ , we arrive at an alternative expression for the Hall conductivity

$$\sigma_H(\omega) = \frac{1}{\mathcal{A}\hbar^2\omega} \text{Im}[\mathcal{J}_x^\dagger G^R(\mathbf{K}, \omega) \mathcal{J}_y], \quad (\text{S30})$$

where  $G^R(\mathbf{k}, \omega)$  is the Fourier transform of the retarded Green's function (in a matrix form)

$$G_{mn}^R(\mathbf{k}, t-t') = -i\hbar^{-1}\theta(t-t')\langle[\hat{\Psi}_{\mathbf{k},m}(t), \hat{\Psi}_{\mathbf{k},n}^\dagger(t')]\rangle. \quad (\text{S31})$$

Within Bogoliubov theory,  $G^R(\mathbf{k}, \omega)$  is given by

$$G^R(\mathbf{k}, \omega) = [(\hbar\omega + i0^+)\tau_z - \mathcal{H}_B(\mathbf{k})]^{-1}. \quad (\text{S32})$$

Now both  $\mathcal{J}$  and  $G^R(\mathbf{k}, \omega)$  can be evaluated perturbatively in terms of the atomic interactions, i.e.,

$$\mathcal{J} = \mathcal{J}^{(0)} + \lambda\mathcal{J}^{(1)} + \lambda^2\mathcal{J}^{(2)} + \dots \quad (\text{S33})$$

$$G^R = G^{(0)} + \lambda G^{(1)} + \lambda^2 G^{(2)} + \dots \quad (\text{S34})$$

where  $\lambda$  is used to keep track of the order of perturbation and will be set to unity at the end of calculation. Substituting the above expansions into Eq. (S30) we find

$$\sigma_H(\omega) = \sigma_H^{(0)}(\omega) + \lambda\sigma_H^{(1)}(\omega) + O(\lambda^2), \quad (\text{S35})$$

where

$$\sigma_H^{(0)}(\omega) = \frac{1}{\mathcal{A}\hbar^2\omega} \text{Im}[\mathcal{J}_x^{(0)} G^{(0)} \mathcal{J}_y^{(0)}] \quad (\text{S36})$$

and

$$\sigma_H^{(1)}(\omega) = \frac{1}{\mathcal{A}\hbar^2\omega} \text{Im}[\mathcal{J}_x^{(0)} G^{(1)} \mathcal{J}_y^{(0)} + \mathcal{J}_x^{(1)} G^{(0)} \mathcal{J}_y^{(0)} + \mathcal{J}_x^{(0)} G^{(0)} \mathcal{J}_y^{(1)}]. \quad (\text{S37})$$

In view of Eq. (S29), in order to obtain the expansion coefficients in Eq. (S33) we need to calculate the condensate wave function  $\langle\hat{\Psi}_{\mathbf{K}}\rangle \equiv \sqrt{N}\Phi_{\mathbf{K}} = \sqrt{N}(\varphi_{s,\mathbf{K}}, \varphi_{p,\mathbf{K}}^+, \varphi_{p,\mathbf{K}}^-)^T$  perturbatively. The latter is the solution to the Gross-Pitaevskii equation

$$([h_0(\mathbf{K}) + V[\Phi_{\mathbf{K}}]]\Phi_{\mathbf{K}} = \mu\Phi_{\mathbf{K}} \quad (\text{S38})$$

where  $V[\Phi_{\mathbf{K}}] = \rho_u \text{diag}(U_s|\varphi_{s,\mathbf{K}}|^2, U_p(|\varphi_{p,\mathbf{K}}^+|^2 + 2|\varphi_{p,\mathbf{K}}^-|^2), U_p(2|\varphi_{p,\mathbf{K}}^+|^2 + |\varphi_{p,\mathbf{K}}^-|^2))$  and  $\mu$  is the chemical potential. Solving the above equation perturbatively in terms of the atomic interactions we find

$$\mu^{(0)} = \epsilon_0(\mathbf{K}); \quad \Phi_{\mathbf{K}}^{(0)} = (\cos \xi_0, \sin \xi_0, 0)^T, \quad (\text{S39})$$

and

$$\begin{aligned} \mu^{(1)} &= U_s \rho_u \cos^4 \xi_0 + U_p \rho_u \sin^4 \xi_0; \\ \Phi_{\mathbf{K}}^{(1)} &= \frac{\rho_u (U_s \cos^2 \xi_0 - U_p \sin^2 \xi_0) \sin \xi_0 \cos \xi_0}{\sqrt{(\epsilon_s - \epsilon_p)^2 + 36|t|^2}} (-\sin \xi_0, \cos \xi_0, 0)^T, \end{aligned} \quad (\text{S40})$$

where  $\sin \xi_0 = 3t/\sqrt{9|t|^2 + (\epsilon_0(\mathbf{K}) - \epsilon_p)^2}$ .

To solve Eq. (S34) we separate  $\mathcal{H}_B(\mathbf{K})$  into the single-particle part

$$\mathcal{H}_0 = \begin{pmatrix} h_0(\mathbf{K}) - \mu^{(0)} & \\ & h_0^*(\mathbf{K}) - \mu^{(0)} \end{pmatrix} \quad (\text{S41})$$

and the part containing interactions

$$\mathcal{H}_I = \begin{pmatrix} g - (\mu - \mu^{(0)}) & g' \\ g' & g - (\mu - \mu^{(0)}) \end{pmatrix}. \quad (\text{S42})$$

The retarded Green's function in Eq. (S32) can then be expanded as

$$G^R(\omega) = G^{(0)} + G^{(0)}\mathcal{H}_I G^{(0)} + G^{(0)}\mathcal{H}_I G^{(0)}\mathcal{H}_I G^{(0)} + \dots \quad (\text{S43})$$

The zeroth order Green's function is simply

$$G^{(0)} = [(\hbar\omega + i0^+)\tau_z - \mathcal{H}_0]^{-1} = \begin{pmatrix} D_\omega & & & \\ & \frac{1}{\hbar\omega + i0^+ - \epsilon_p + \mu^{(0)}} & & \\ & & D_{-\omega} & \\ & & & \frac{1}{-\hbar\omega - i0^+ - \epsilon_p + \mu^{(0)}} \end{pmatrix}, \quad (\text{S44})$$

where

$$D_{\pm\omega} = \begin{pmatrix} \pm\hbar\omega \pm i0^+ - \epsilon_s + \mu^{(0)} & -3t \\ -3t & \pm\hbar\omega \pm i0^+ - \epsilon_p + \mu^{(0)} \end{pmatrix}^{-1}.$$

The first order correction takes the form of

$$G^{(1)} = \begin{pmatrix} D_\omega D_a D_\omega & 0 & D_\omega D_x D_{-\omega} & 0 \\ 0 & \frac{2\rho_u U_p \sin^2 \xi_0 - \mu^{(1)}}{(\hbar\omega + i0^+ - \epsilon_p + \mu^{(0)})^2} & 0 & 0 \\ D_{-\omega} D_x D_\omega & 0 & D_{-\omega} D_a D_{-\omega} & 0 \\ 0 & 0 & 0 & \frac{2\rho_u U_p \sin^2 \xi_0 - \mu^{(1)}}{(-\hbar\omega - i0^+ - \epsilon_p + \mu^{(0)})^2} \end{pmatrix}, \quad (\text{S45})$$

where

$$D_a = \begin{pmatrix} 2\rho_u U_s \cos^2 \xi_0 - \mu^{(1)} & \\ & 2\rho_u U_p \sin^2 \xi_0 - \mu^{(1)} \end{pmatrix}; D_x = \begin{pmatrix} \rho_u U_s \cos^2 \xi_0 & \\ & \rho_u U_p \sin^2 \xi_0 \end{pmatrix}.$$

Combining Eq. (S29), (S36), (S39) and (S44), we find the non-interacting Hall conductivity as

$$\sigma_H^{(0)}(\omega) = \frac{N}{\hbar\mathcal{A}} \frac{3a^2 |t|^2 \cos^2 \xi_0}{2[\Delta^2 - (\hbar\omega)^2]} \quad (\text{S46})$$

where  $\Delta = \epsilon_p - \mu^{(0)}$  is the band gap at  $\mathbf{K}$  point between the bottom and the second non-interacting bands. At zero frequency we obtain

$$\sigma_H^{(0)}(0) = \frac{N}{\hbar\mathcal{A}} \Omega_0^{(0)}(\mathbf{K}), \quad (\text{S47})$$

where

$$\Omega_0^{(0)}(\mathbf{K}) = \frac{3a^2 |t|^2 \cos^2 \xi_0}{2\Delta^2} \quad (\text{S48})$$

is precisely the Berry curvature at  $\mathbf{K}$  point of the bottom non-interacting band. Combining Eq. (S29), (S37), (S40) and (S45), we find the first order correction to the Hall conductivity due to atomic interactions

$$\sigma_H^{(1)}(\omega) = -\frac{N}{\hbar\mathcal{A}} 3a^2 |t|^2 \cos^2 \xi_0 \times \left\{ \frac{\rho_u (U_s \cos^2 \xi_0 - U_p \sin^2 \xi_0) \sin^2 \xi_0}{(\Delta^2 - \hbar^2 \omega^2) \sqrt{(\epsilon_s - \epsilon_p)^2 + 36|t|^2}} + \frac{\Delta [\rho_u U_p \sin^2 \xi_0 (1 + \cos^2 \xi_0) - \rho_u U_s \cos^4 \xi_0]}{(\Delta^2 - \hbar^2 \omega^2)^2} \right\}. \quad (\text{S49})$$

In the dc limit and with  $\epsilon_s = \epsilon_p$ , we have  $\Delta = 3|t|$  and  $\cos^2 \xi_0 = 1/2$  and this expression reduces to

$$\sigma_H^{(1)}(0) = -\frac{N}{\hbar\mathcal{A}} \frac{\rho_u a^2}{144|t|} (5U_p - U_s). \quad (\text{S50})$$

\* xuzf@sustech.edu.cn

† wuzg@sustech.edu.cn

- [1] X.-Q. Wang, G.-Q. Luo, J.-Y. Liu, W. V. Liu, A. Hemmerich, and Z.-F. Xu, Evidence for an atomic chiral superfluid with topological excitations, *Nature* **596**, 227 (2021).  
 [2] N. Marzari, A. A. Mostofi, J. R. Yates, I. Souza, and D. Vanderbilt, Maximally localized wannier functions: Theory and applications, *Rev. Mod. Phys.* **84**, 1419 (2012).